Sparse wire grid 3D printed patch antenna

Manh Tuan Nguyen
Department of Television and Control
Tomsk State University of Control Systems and Radioelectronics
Tomsk, Russia
nguyen.t.2213-2022@e.tusur.ru

Adnan F. Alhaj Hasan
Department of Television and Control
Tomsk State University of Control Systems and Radioelectronics
Tomsk, Russia
alkhadzh@tusur.ru

Talgat R. Gazizov
Department of Television and Control
Tomsk State University of Control Systems and Radioelectronics
Tomsk, Russia
talgat.r.gazizov@tusur.ru

***Abstract*—Currently, the development of 5G networks brings a number of challenges for the design and deployment of new antenna types. In urban environments, antennas must not only have high performance, but also lower mass, as well as the ability to integrate into the environment and be invisible in the general landscape. One of the recently witnessed solutions is the design of wire grid antennas. Based on the wire grid antenna, a sparse structure with lower mass can be designed while maintaining the antenna characteristics. In this paper, we have modeled a wire grid patch antenna in various computer-aided design systems. The simulation results are compared with each other and with the measured results of the antenna model fabricated using 3D printing technology. In addition, we also applied different approaches to the original structure in order to create sparse wire grid structures. The main antenna characteristics obtained for these sparse structures are compared with those for the original one. The compared results showed a good agreement. The created sparse structures had less mass as well as memory and time for subsequent simulations compared to the original one. Moreover, the resulting sparse structures have unfamiliar shapes, which allows them to be easily integrated into various locations without compromising the urban landscape.**

Keywords—wire-grid, sparse antennas, 3D printed patch antennas, method of moments, optimal current grid approximation, 5G network technology, hidden antenna.

I. Introduction

Metropolitan environments are characterized with high population density, complex architectural designs, and obstacles such as buildings, trees, and vehicles. Thus, 5G networks in such environments faces a number of challenges related to antenna design and deployment [1, 2]. Since these networks support modern applications such as self-driving cars, smart sensors, and mobile medical technologies, their antennas need to satisfy special requirements. It must provide wide coverage and best data transmission performance in high-density areas and yet to concentrate radio waves to overcome obstacles while at the same time to be inconspicuous and integrated into the environment [3]. Smart and space-saving manner in antenna design may integrate them into existing infrastructure, such as on electrical poles, buildings and even billboards or building windows.

One of the recently witnessed solutions of these problems is the development of wire grid (WG) antennas [4, 5]. They have less mass than traditional antennas and can be easily installed in various locations without affecting the urban landscape. The rapid development of 3D printing technology in tandem with its utilization for designing WG antennas offer many outstanding advantages in 5G antenna deployment [6–8]. This allows designers to precisely and accurately create antennas in a variety of complex shapes and sizes while minimizing manufacturing errors and costs.

However, antennas must be carefully modeled in various computer-aided design (CAD) systems before fabrication. Currently, there are many CAD systems with different numerical methods for modeling WG antennas, such as CST [9] with the time domain finite difference and element methods, 4NEC2 [10] with the method of moments (MoM) and triangular basis functions, TALGAT [11] with MoM and pulse basis functions. Each CAD system has its own advantages and disadvantages. Therefore, a comparative analysis of WG antenna simulation results in different CAD systems is necessary during their design process.

According to WG approach, solid structures can be replaced with a grid of electrically connected wires through which surface currents can find their way. Although the resulting WG structure has a smaller mass compared to the solid one, a significant number of wires in the grid is still unnecessary. Thus, it is reasonable to create a grid with wires that follow the current path. Based on this, an approach to eliminate these unnecessary wires, called optimal current grid approximation (OCGA), was proposed in [12]. The principal concept behind OCGA is to eliminate wires with small current magnitude, since their contribution to the radiation is small. Once the grid current distribution is obtained, all current magnitudes must be normalized to either their maximum or average values, and then OCGA eliminates all wires with normalized current magnitudes less than a given level, known as the Grid Element Elimination Tolerance (GEET). This value can be chosen depending on the manufacturer's requirements.

However, as the GEET value increases, unconnected (free) wires to the structure appear. This leads to break the grid electrical paths which makes it difficult to fabricate the WG antenna. Therefore, two OCGA modifications were proposed in [13] to solve this problem: the "eliminating" OCGA (EOCGA) and the "near-connecting" OCGA (NCOCGA). The principle of the EOCGA approach is to eliminate all free wires, while NCOCGA is to rebuild only the necessary wires to reconnect the free ones to the structure. OCGA and their modifications allow the design of sparse WG antennas with lower mass while maintaining the required antenna performance. In addition, the resulting sparse structures after OCGA have a variety of shapes and sizes compared to conventional ones, which allows them to be placed in different locations in the urban environment.

Thus, the design of new sparse OCGA-based WG antennas that have lower mass, can be fabricated using 3D printing technology and hidden in the environment without affecting the overall landscape is very important to satisfy the growing demands of the 5G applications. Therefore, the main purpose of this paper is to compare the hidden WG patch

This research was funded by the Ministry of Science and Higher Education of the Russian Federation project FEWM-2023-0014.

XXX-X-XXXX-XXXX-X/XX/$XX.00 ©20XX IEEE

antenna characteristics obtained experimentally and numerically in different CAD systems and then apply the OCGA and its modifications to generate its novel sparse WG structure.

This study is organized as follows: Section II provides a detailed description of the WG patch antenna geometrical and numerical models in different CAD systems. The simulation results obtained are compared with each other and with those measured for a 3D printing antenna model. Section III presents the results of applying OCGA and its modifications to the original WG structure. The GEET dependences of the antenna characteristics after applying different approaches are provided. In addition, examples of sparse structures at specific GEET value are also shown. The sparse structures results are compared with each other and with those of the original one. Finally, Section IV summarizes the research conclusions.

II. WG Patch Antenna: Modeling and Comparison

To achieve the purpose of this work, the WG patch antenna from [14] is selected. It is designed for 5G applications and works at the frequency of 2.6 GHz (λ=115.4 mm). Its structure is composed of two main parts: the patch grid and the ground plane grid. Their isometric view is shown in Fig. 1, while their main geometric parameters are given in Table I.

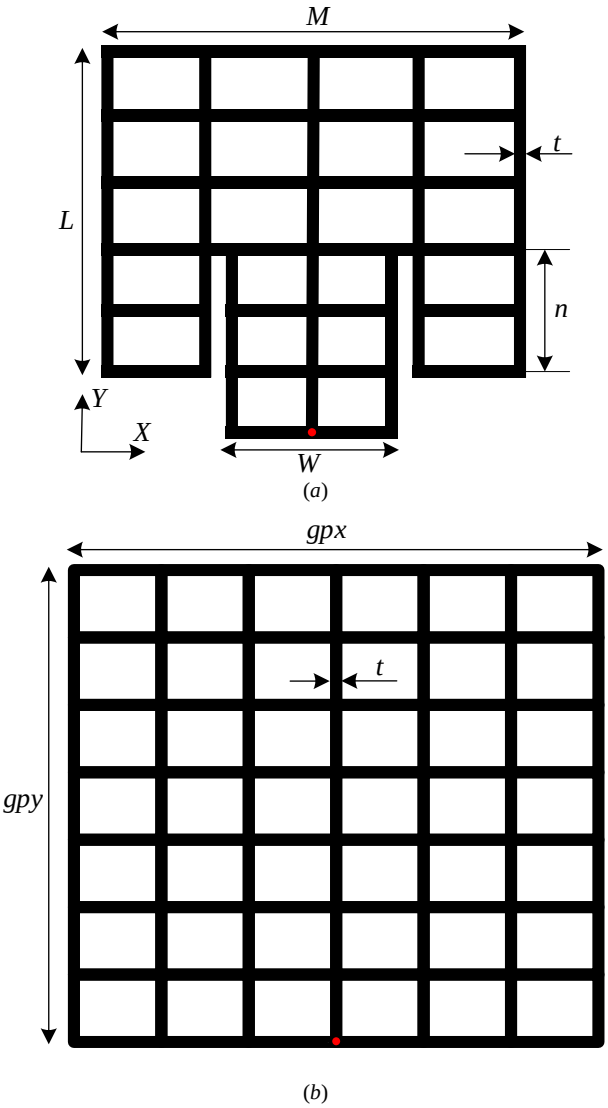

Fig. 1. WG antenna structure: patch (*a*) and ground plane (*b*) grids.

TABLE I. The Patch Antenna Geometric Parameters [14]

L, mm	*M*, mm	*W*, mm	*n*, mm	*t*, mm	*gpx*, mm	*gpy*, mm
46.2	46.2	15.6	16.3	1	64.4	64.4

The grids are placed in the OXY plane at a distance h=3 mm along the OZ axis and fixed by dielectric pins to provide mechanical support to the structure. According to the researchers in [15], it is recommended to choose a WG ground plane cell size in the range of 0.05λ to 0.1λ (5.77–11.54 mm) to achieve a good electromagnetic field shielding. Therefore, the ground plane grid is divided into 6 parts along the OX axis and 7 parts along the OY axis, which corresponds to a size of 0.09λ×0.08λ (*gpx*/6=10.73 mm and *gpy*/7=9.2 mm).

To model the WG patch antenna in TALGAT and 4NEC2, the wire radius (R_W) is taken equal to the half of the metallic grid thickness (t) and is equal to 0.5 mm. To excite the antenna, a wire with a potential difference of 1 V is placed along the OZ axis and directly connected the patch grid to the ground plane one at the excitation point (red points in Fig. 1). It has a length of h and a radius (r_S) of 0.46 mm. All wires in the grid including the excitation one are presented by one segment. The authors of [14] modeled this antenna in CST and then manufactured it using the 3D printing technology. All the WG patch antenna models: 3D printed and in CST ([14]), and in 4NEC2 and TALGAT (ours) are presented in Fig. 2.

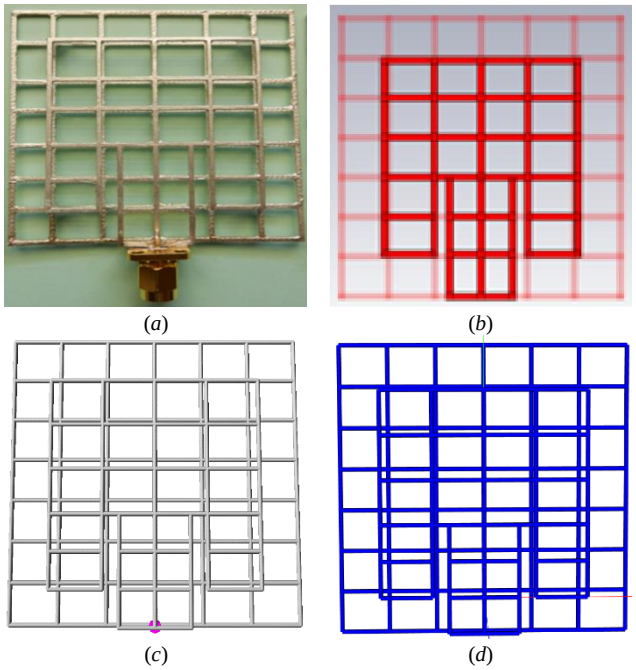

Fig. 2. WG patch antenna models: 3D printed [14] (*a*), designed in CST [14] (*b*), in 4NEC2 (*c*), and in TALGAT (*d*).

The main antenna characteristics obtained in each CAD were compared with each other as well as with the measured ones for the manufactured model. Fig. 3 shows a comparison in the frequency range of 2–3 GHz of the antenna reflection coefficient ($|S_{11}|$) and its realized gain $G_r=G^*(1-|S_{11}|^2)$ which is the gain value taking into account the mismatch loss. It can be noticed from Fig. 3*a* that the CST simulation results give an operational frequency centered at 2.6 GHz. The measured and simulated in TALGAT results are close and give a resonance (at 2.64 GHz) with a small difference from the target frequency of 2.6 GHz. 4NEC2 results give a resonance at 2.34 GHz which has the largest discrepancy from the measured and desired values. In addition, the lowest value of $|S_{11}|$ at the resonant frequency is obtained in TALGAT (–

40.1 dB), followed by in CST (–19,8 dB), experimentally (–26.2 dB) and in 4NEC2 (–12.4 dB). When considering the G_r value in Fig. 3*b*, it can be noticed that the differences between the results obtained in CST and TALGAT comparing to the measured ones are less noticeable compared with the differences of results obtained in 4NEC2 from the measured ones. In details, at the frequency of 2.6 GHz, the highest G_r value obtained in TALGAT (9.78 dB), followed by CST (7.9 dB), experimentally (4.92 dB), and 4NEC2 (–7.03 dB). The simulation results in CST and TALGAT are acceptable comparing to the measured ones and their discrepancies are explained by the difference between the 3D printed and simulated antenna models. The antenna directivity is also considered comparing its radiation patterns (RP) at 2.6 GHz in the *E* and *H* planes (Fig. 4).

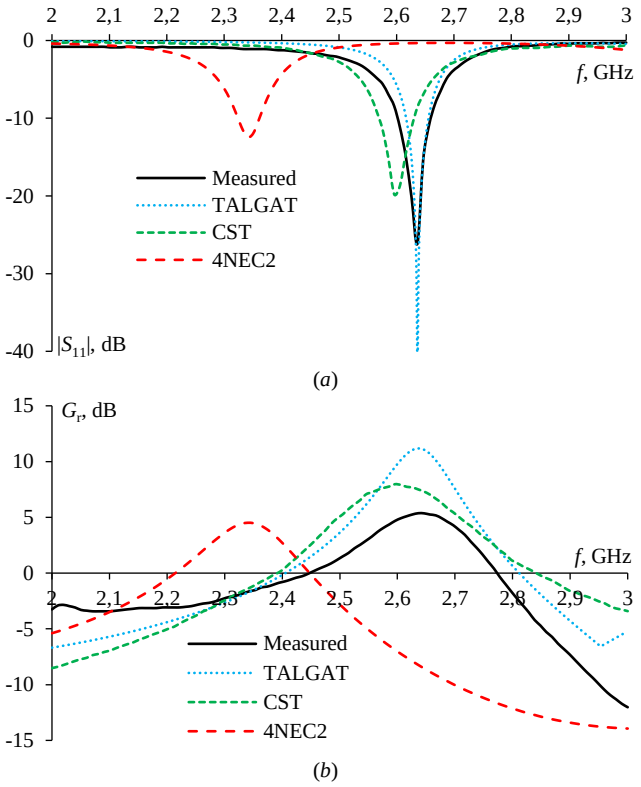

Fig. 3. WG patch antenna $|S_{11}|$ (*a*) and G_r (*b*) obtained experimentally [14] and numirically in CST [14], TALGAT and 4NEC2.

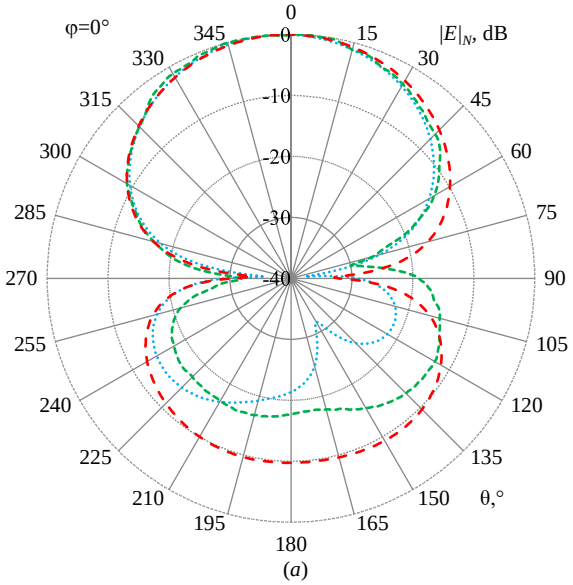

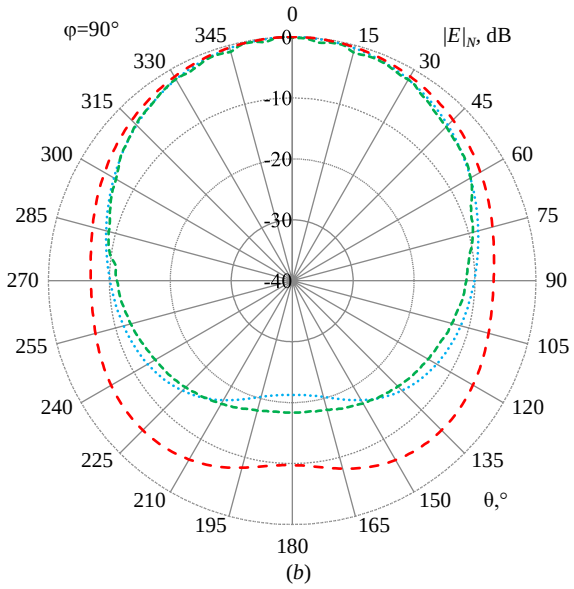

Fig. 4. WG patch antenna RPs obtained in CST [14] (---), TALGAT (···) and 4NEC2 (– –) at 2.6 GHz in *E* (*a*) and *H* (*b*) planes.

According to the RPs obtained in Fig. 4, it can be noticed that the results obtained in CST and TALGAT have a good agreement in the main radiation directions in the *E* and *H* planes. In details, the obtained beamwidths at –3 dB (BW) in the *E* and *H* planes in TALGAT are 62.5º/77º and in CST 66.5º/74º. Meanwhile, the BW obtained in 4NEC2 are 68º/94º. Furthermore, when considering the back lobe level (BLL), the results obtained in TALGAT also demonstrate a good agreement with those in CST. Specifically, the BLL obtained in the *E* and *H* planes in TALGAT are –14.35/–21.28 dB, while in CST are –12.720/–18.34 dB and in 4NEC2 are –9.22/–9.73 dB.

The comparison demonstrated that the TALGAT results are in good agreement with those obtained in CST and experimentally for the 3D printed patch antenna. They also showed effectiveness of MoM with pulse basis functions in modeling WG antennas. Therefore, to obtain the sparse antenna structure, the WG structure in TALGAT will be used as the original one in order to apply the OCGA, EOCGA and NCOCGA approaches on it.

III. WG Sparse Structures

The sparse structures obtained after applying OCGA, EOCGA and NCOCGA are mainly depend on the current distribution in the WG and the GEET value. According to OCGA, the current values along the wires can be normalized to the maximum or the average current magnitudes. In the case of a patch antenna, the excitation source is connected directly to the structure, which results in a much higher current in the wires near it than others. Therefore, we normalized the current magnitudes to their average value. Then the normalized magnitudes are compared with the GEET value. Wires with normalized current magnitudes less than the GEET value are eliminated from the original structure. As a result, the obtained sparse structure only consists of wires with normalized current magnitudes higher than the GEET value.

As the GEET value changes, the number of wires eliminated from the grid can be changed differently after applying the considered approaches. Fig. 5 shows the GEET dependence of the remaining wires number for different sparse structures. Moreover, changing the structure wires

number is also directly influence the resulting antenna mass and its modeling costs such as the required time and memory for each simulation. The GEET dependences of the antenna mass reduction, and time and memory reduction on subsequent simulations are shown in Fig. 6.

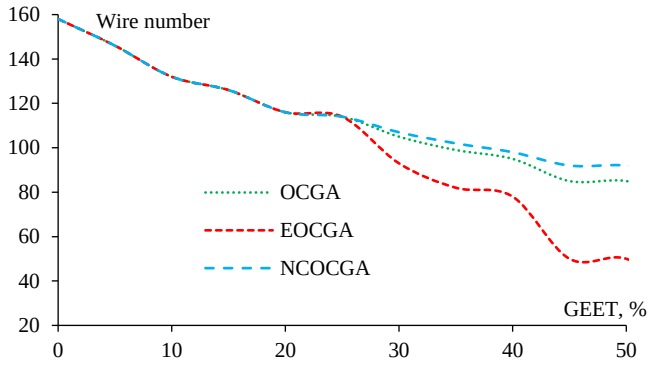

Fig. 5. GEET dependences of the total number of remaining wires in the sparse WG patch antenna after OCGA, EOCGA, and NCOCGA.

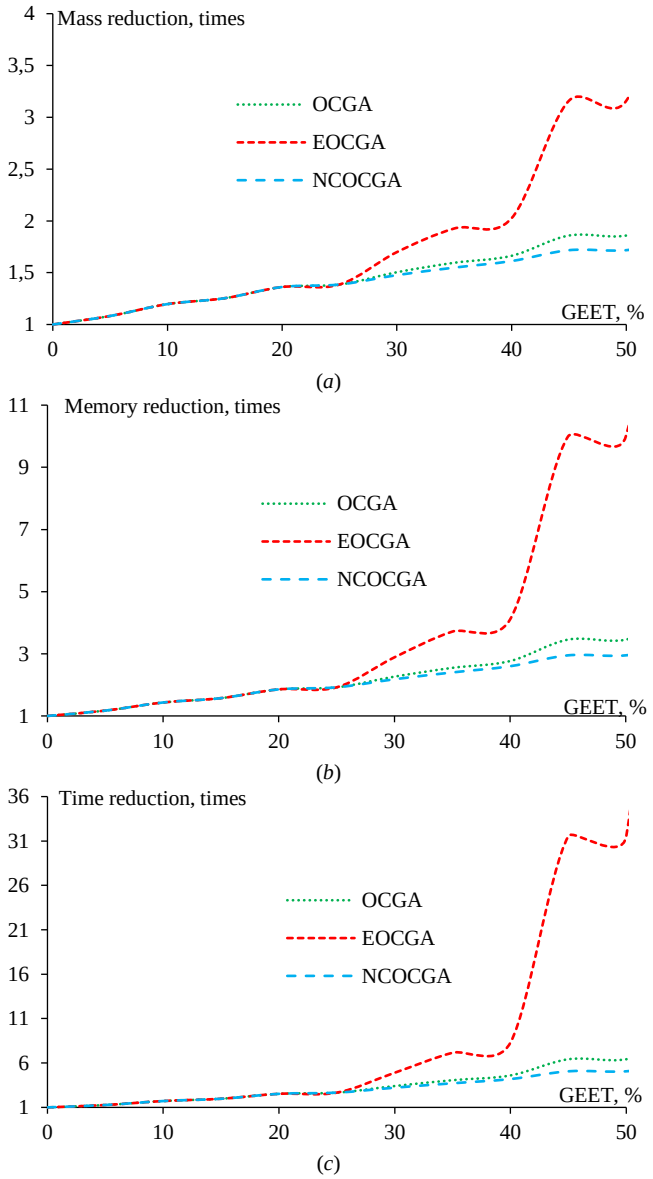

Fig. 6. GEET dependences of the sparse WG patch antenna mass (*a*), memory (*b*) and time (*c*) reduction on subsequent simulations after OCGA, EOCGA, and NCOCGA.

Fig. 5 show that when the GEET value increases, the number of remaining wires decreases. This leads to a reduction in the antenna mass, time and memory required when using the sparse structure instead the original one for subsequent simulation (Fig. 6). Furthermore, it can be observed that after applying NCOCGA, the number of remaining wires is always higher than after OCGA and EOCGA. This is because NCOCGA restores some wires after OCGA to connect the free wires to the structure in order to maintain the integrity of the WG, while EOCGA removes these free wires. Therefore, the reduction in antenna mass, time and memory for subsequent simulation after EOCGA is always higher than that after NCOCGA and OCGA. As the number of wires changes, the antenna characteristics also change, which must be carefully considered before selecting a GEET value. The voltage standing wave ratio (VSWR), G_r, $|S_{11}|$ and absolute input impedance $|Z|$ were compared at 2.6 GHz after applying OCGA, EOCGA and NCOCGA at different GEET values that varied from 0 to 50% (Fig. 7).

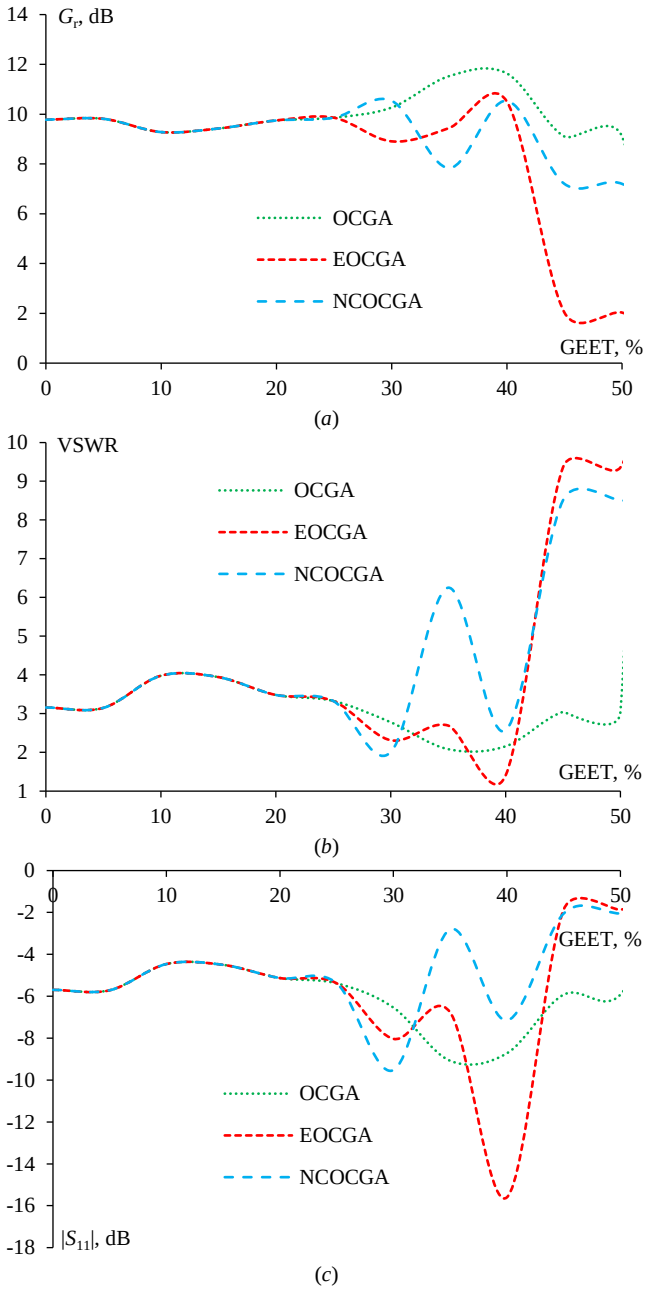

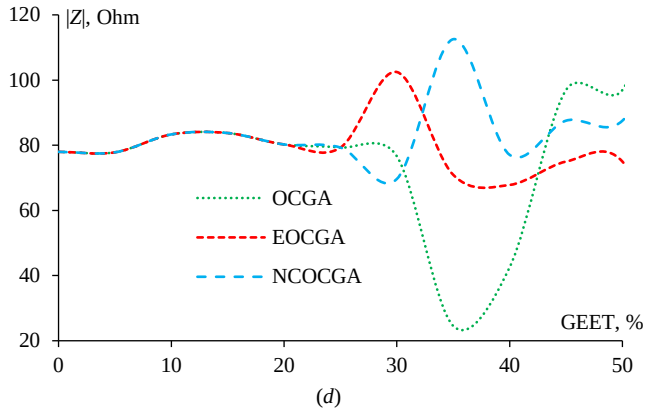

Fig. 7. GEET dependences of the obtained G_r (*a*), VSWR (*b*), $|S_{11}|$ (*c*), and $|Z|$ (*d*) of the sparse WG antenna after OCGA, EOCGA, and NCOCGA

The compared results in Fig. 7 show that when the GEET<25%, the main sparse antenna characteristics obtained after different approaches have no differences and practically do not differ from the original structure (at GEET=0%). For GEET>25%, the difference becomes more noticeable and requires careful consideration. As an example, we chose the GEET value of 30% and analyzed in detail the performance of sparse antennas in the operating frequency range. To show the working principle of the considered approaches, the original WG structure with its current distribution and the obtained sparse structures after OCGA, EOCGA and NCOCGA are shown together in Fig. 8.

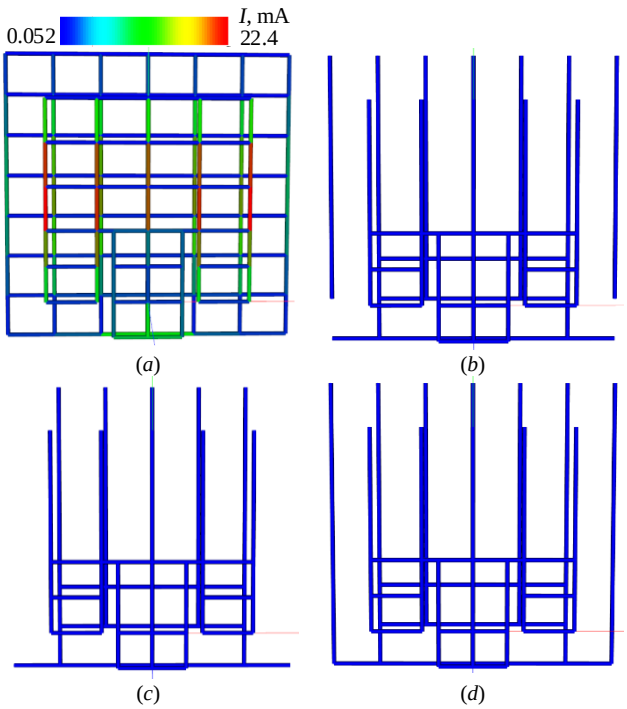

Fig. 8. Current distribution on the original WG structure (*a*). The obtained sparse structures after OCGA (*b*), EOCGA (*c*) and NCOCGA (*d*).

Fig. 8*b* shows that all wires with low current magnitudes in the original WG structure (blue wires in Fig. 8*a*) were eliminated after OCGA. However, the resulting sparse structure have some free wires. EOCGA eliminated these free wires and created another sparse structure in Fig. 8*c*. While NCOCGA restored some wires necessary to create connections between the free ones and the structure (Fig. 8*d*). The total wire number of the original structure is N=158, while its values after applying OCGA, EOCGA and NCOCGA are N_O=105, N_E=93, N_N=107, respectively. As is known, the basic time required to solve a system of linear algebraic equations using the Gaussian elimination is proportional to the third degree of its order $O(N)^3$, while the required memory is proportional to the square of its order $O(N)^2$. The reductions of antenna mass, memory and time for further simulation after OCGA are 1.50, 2.26, 3.41 times, after EOCGA are 1.70, 2.89, 4.90 times and after NCOCGA are 1.48, 2.18, 3.22 times, respectively. Moreover, these structures have unfamiliar antenna shapes. Therefore, it is possible to utilize them in applications where hidden antenna are required without disturbing the overall landscape of the environment.

To verify the performance of the obtained sparse antennas after OCGA, EOCGA and NCOCGA, their main characteristics are compared with those for the original structure in the frequency range of 2–3 GHz (Fig. 9). In addition, the RPs of the sparse structures were also compared with those of the original structure in the *E* and *H* planes at 2.6 GHz (Fig. 10). The compared results were analyzed at 2.6 GHz and at the resonances frequencies and summarized in Tables II and III, respectively.

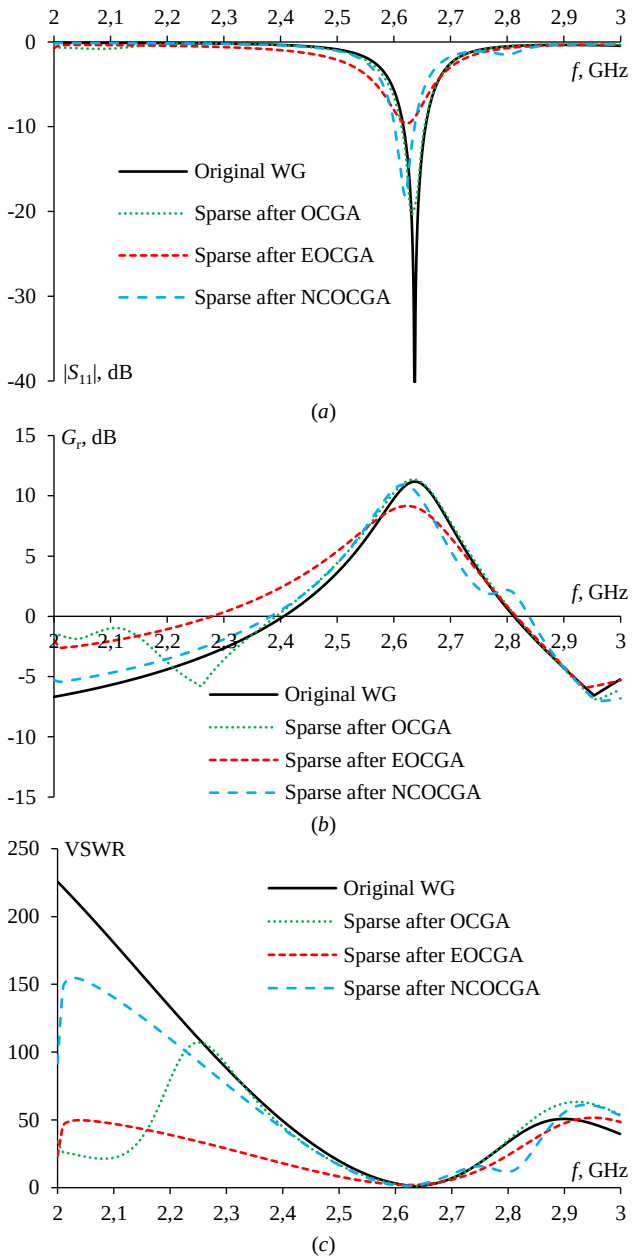

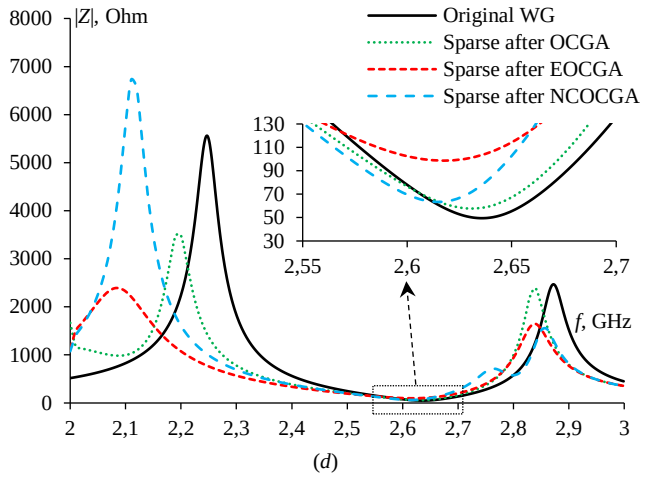

(*d*)

Fig. 9. Frequency dependences of the obtained $|S_{11}|$ (*a*), G_r (*b*), VSWR (*c*), and $|Z|$ (*d*) for the original and sparse WG patch antennas after OCGA, EOCGA, and NCOCGA.

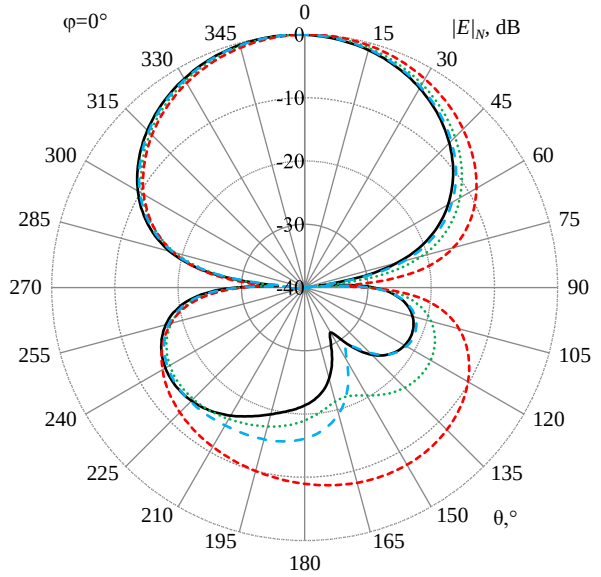

(*a*)

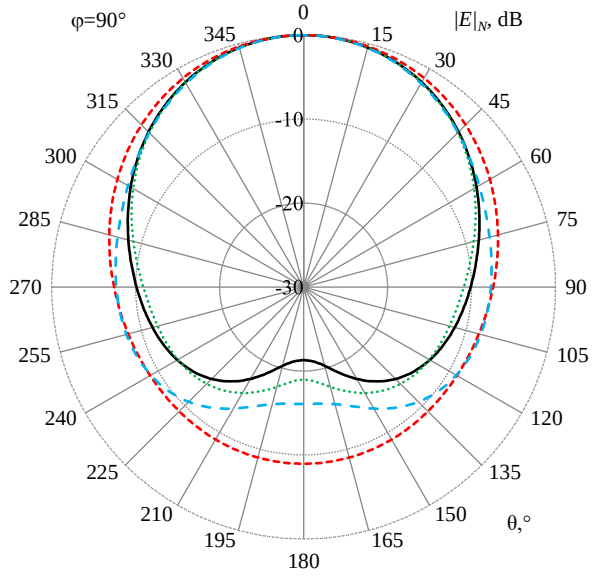

(*b*)

Fig. 10. Obtained RPs of the original (—) and sparse WG patch antennas after OCGA (····), EOCGA (---), and NCOCGA (– –) in *E* (*a*) and *H* (*b*) planes at 2.6 GHz.

TABLE II. MAIN CHARACTERISTICS OF PATCH ANTENNA DIFFERENT WG MODELS AT 2.6 GHZ

Models	**$\|S_{11}\|$, dB**	**G_r, dB**	**VSWR**	**$\|Z\|$, Ohm**	**BLL (*E*/*H*), dB**	**BW (*E*/*H*), °**
Original WG	–5.69	9.78	3.16	77.98	–14.35/ –21.28	62.5/77
Sparse OCGA	–6.54	10.27	2.78	76.61	–14.99/ –18.96	63.5/76
Sparse EOCGA	–8.03	8.91	2.31	102.46	–7.64/ –8.95	68/95
Sparse NCOCGA	–9.53	10.54	2.00	69.64	–14.47/ –16.07	62.5/74

TABLE III. MAIN CHARACTERISTICS OF PATCH ANTENNA DIFFERENT WG MODELS AT THIER RESONANCES FREQUENCIES

Models	**$f_{resonance}$, GHz**	**$\|S_{11}\|$, dB**	**G_{real}, dB**	**VSWR**	**$\|Z\|$, Ohm**
Original WG	2.64	-40.10	11.18	1.02	49.52
Sparse OCGA	2.63	-20.20	11.34	1.22	57.72
Sparse EOCGA	2.62	-9.58	9.15	1.99	98.77
Sparse NCOCGA	2.62	-18.10	10.93	1.28	64.21

The comparison demonstrates that the antenna characteristics of the sparse structures after OCGA and NCOCGA have small differences from those of the original structure, while the sparse structure after EOCGA has a larger difference. Fig. 9 shows that the resonance frequency of the sparse structures is closer to the target frequency of 2.6 GHz from its value for the original structure. Table II show that at 2.6 GHz the main antenna characteristics of the sparse structures after OCGA and NCOCGA are even a little better than those for the original structures, such as $|S_{11}|$, G_{real}, VSWR and $|Z|$. However, at resonances frequencies, the obtained characteristics of the sparse structures are slightly worse than those for the original one. These differences are not significant and are acceptable considering the reduction in antenna mass and time and memory for subsequent simulations compared to the original structure. These comparisons have shown the possibility of using sparse structures instead of the original one with controlled: characteristics accuracy, mass reduction, as well as time and memory reduction for subsequent simulations.

IV. CONCLUSION

In summary, this paper has comprehensively analyzed the modeling results of the WG patch antenna in different CAD systems. The obtained results showed the effectiveness of MoM with pulse basis function in modeling WG antenna since its results are the closer to the measured ones from the others. Sparse structures obtained after applying different approaches were analyzed. The GEET dependence of the antenna characteristics after their applying are provided and analyzed. Moreover, the characteristics were also compared at a specific GEET value and showed small differences from those for the original structure. These differences may be considered acceptable taking into account the reduction in mass as well as memory and time required on further simulations.

In addition, the resulting sparse antenna structures after applying these approaches have different shapes and sizes compared to the original one. They may resemble fences, billboards or window frames of buildings. Therefore, it is possible to utilize them in applications where hidden antenna are required without disturbing the overall landscape of the environment. With the widespread deployment of sparse

antennas, it is becoming possible to provide reliable 5G network data transmission along with maintaining healthy and beautiful environment.

REFERENCES

[1] N. Kishore and A. Senapati, “5G smart antenna for IoT application: A review,” International Journal of Communication Systems, vol. 35, no. 13, p. e5241, Sep. 2022, doi: 10.1002/DAC.5241. [CrossRef].

[2] W. Hong, K. -H. Baek and S. Ko, “Millimeter-Wave 5G Antennas for Smartphones: Overview and Experimental Demonstration,” in IEEE Transactions on Antennas and Propagation, vol. 65, no. 12, pp. 6250–6261, Dec. 2017, doi: 10.1109/TAP.2017.2740963. [CrossRef].

[3] A. A. Vaganova, N. N. Kisel and A. I. Panychev, "Simulation Model of 5G Coverage in Urban Areas," 2019 Radiation and Scattering of Electromagnetic Waves (RSEMW), Divnomorskoe, Russia, 2019, pp. 372-375, doi: 10.1109/RSEMW.2019.8792791. [CrossRef].

[4] T. R. Gazizov, A. A. Hasan and M. T. Nguyen, "A Simple Modeling Methodology for Creating Hidden Antennas," 2023 International Conference on Industrial Engineering, Applications and Manufacturing (ICIEAM), Sochi, Russian Federation, 2023, pp. 1080-1084, doi: 10.1109/ICIEAM57311.2023.10139026. [CrossRef].

[5] S. Ahn and H. Choo, "A Systematic Design Method of On-Glass Antennas Using Mesh-Grid Structures," in IEEE Transactions on Vehicular Technology, vol. 59, no. 7, pp. 3286-3293, Sept. 2010, doi: 10.1109/TVT.2010.2053227.

[6] G. L. Huang, S. G. Zhou, C. Y. D. Sim, T. H. Chio and T. Yuan, “Lightweight Perforated Waveguide Structure Realized by 3-D Printing for RF Applications,” in IEEE Transactions on Antennas and Propagation, vol. 65, no. 8, pp. 3897–3904, Aug. 2017. [CrossRef].

[7] M. A. Colgan and M. S. Mirotznik, “Design and Fabrication of 3D Wire Grid Antenna An Integrated Method for Optimization in Constrained Volumes,” 2020 IEEE International Symposium on Antennas and Propagation and North American Radio Science Meeting, Montreal, QC, Canada, 2020, pp. 1553–1554, doi: 10.1109/IEEECONF35879.2020.9329555. [CrossRef].

[8] D. Helena, A. Ramos, T. Varum and J.N. Matos, “The Use of 3D Printing Technology for Manufacturing Metal Antennas in the 5G/IoT Context,” Sensors, vol. 21, no. 10, p. 3321, 2021, doi: 10.3390/s21103321 [CrossRef].

[9] CST Studio Suite. Available online: https://www.3ds.com/ru/produkty-i-uslugi/simulia/produkty/cst-studio-suite/ (accessed on 15.03.2024)

[10] NEC based antenna modeler and optimizer. Available online: https://www.qsl.net/4nec2/ (accessed on 15.03.2024)

[11] TALGAT system. Available online: https://talgat.org/talgat-software/ (accessed on 15.03.2024)

[12] A. Alhaj Hasan, T. M. Nguyen, S. P. Kuksenko and T. R. Gazizov, “Wire-grid and sparse MoM antennas: past evolution, present implementation and future possibilities,” Symmetry, 2023, vol. 15(2), p. 378. doi: 10.3390/sym15020378 [CrossRef].

[13] A. A. Hasan, T. M. Nguyen and T. R. Gazizov, “Novel MoM-Based Approaches for Generating Wire-Grid Sparse Antenna Structures," 2023 IEEE 24th International Conference of Young Professionals in Electron Devices and Materials (EDM), Novosibirsk, Russian Federation, 2023, pp. 570–576, doi: 10.1109/EDM58354.2023.10225219. [CrossRef].

[14] Inclán-Sánchez L. “Performance Evaluation of a Low-Cost Semitransparent 3D-Printed Mesh Patch Antenna for Urban Communication Applications” Electronics, vol. 13, no. 1. pp. 153, 2024, doi: 10.3390/electronics13010153 [CrossRef].

[15] S. H. Kang and C. W. Jung, “Transparent Patch Antenna Using Metal Mesh,” IEEE Transactions on Antennas and Propagation, vol. 66, no. 4, pp. 2095-2100, April 2018, doi: 10.1109/TAP.2018.2804622. [CrossRef].